Fiber Field-Effect Device Via In Situ Channel Crystallization

By *Sylvain Danto, Fabien Sorin, Nicholas D. Orf, Zheng Wang, Scott A. Speakman, John D. Joannopoulos,* and *Yoel Fink**

The development of glassy chalcogenide compounds has proceeded in two principle directions. On one hand chalcogenide compositions are selected to have high glass forming ability. These materials can be processed over a broad range of temperatures without inducing parasitic devitrification that reduces both their mechanical strength and optical transparency. S- and Se-based glasses, whose ring-like and long chain polymeric configurations are especially suited for forming stable amorphous phases, are typical materials used in mid-IR thermal imaging lenses, evanescent-wave sensors and high-power laser delivery fibers.[1] In the other research direction, relatively unstable compositions are designed to undergo glass-crystal phase changes under external stimuli while producing drastic modifications in their electrical or optical properties. For this purpose, Te-based materials, with their relatively short polymeric chains and semimetallic character, are currently attracting considerable interests in the fields of optical data storage and non-volatile memory.[2]

Glassy chalcogenide compounds have been shown to co-draw with metals and polymeric insulators into tens-of-meters-long, light-weight and flexible fibers with unusual functionalities.[3–7] To date, however, these multimaterial fibers exhibit limited electrical performance due to the use of thermally stable glassy semiconductors. Indeed, amorphous materials exhibit a continuous change in viscosity with respect to the temperature between the solid and liquid states necessary for thermal drawing, but this disordered state also results in high densities of electronic defects and poor electrical properties. Here for the first time, we exploit two seemingly incompatible properties of a chalcogenide glass in a single fiber device: high glass stability for thermal drawing and phase-change ability for enhanced electrical transport properties. The in situ phase transition of the semiconductor from the amorphous to crystalline state holds great promise for building active electric devices into single multimaterial fibers. As a concrete example, we present the first meters-long fiber-based p-channel field-effect device, demonstrating that through the process of in situ phase transition, the Fermi level of the semiconductor is unpinned and the mobility of the crystalline semiconductor is substantially improved over the amorphous state.

To alleviate the limitation imposed by the electrical properties of amorphous semiconductors, we thermally anneal the fibers to drive the glass from the metastable amorphous state to the equilibrium crystalline state. This in situ crystallization approach imposes additional requirements on the materials besides their compatibility with the co-drawing process. As before, the amorphous semiconductor must resist crystallization during fiber drawing. Additionally, it must now be not so stable that the extended time to achieve thermal crystallization becomes experimentally inconvenient. Semiconductor glasses in the pseudo-binary system $As_{40}Se_{60}$-$As_{40}Te_{60}$ reconcile these two opposing requirements.[8–11] These glasses are compatible with a thermal co-drawing process at low Te content while their crystallization is significantly promoted as the content of Te increases.[6,8–10] The glass $As_{40}Se_{52}Te_8$ was found to be a good composition because of its use as an amorphous semiconductor for thermal drawing and its ability to be subsequently crystallized in situ.

To demonstrate this new post-drawing crystallization scheme, we fabricated fibers with a simple solid-core structure (**Figure 1**). Macroscopic preforms consisting of an $As_{40}Se_{52}Te_8$ glass rod (T_g = 165 °C) contacted by four tin electrodes (T_m = 232 °C) and surrounded by a polyethersulfone (PES) cladding (T_g = 225 °C) were consolidated at 260 °C for ~30 min (Figure 1a) and thermally drawn at ~290 °C into tens of meters of fiber (Figure 1b) (see Experimental Section). The semiconducting glass was then converted to the crystalline phase by thermal annealing (Figure 1c). Annealing was fixed at 208 °C to balance the need to occur at temperatures significantly exceeding the glass transition of the semiconductor to promote crystallization but also be below the T_g of the polymer cladding and the T_m of the electrodes to preserve the structural integrity and the mechanical properties of the fibers during annealing. In Figure 1c, a scanning electron microscopy (SEM) image of a fiber cross-section clearly shows crystallites within the semiconductor region (annealed for 40 days to maximize the visibility of the crystalline domains).

Semiconductor crystallinity was further confirmed by X-ray diffraction (XRD) and differential scanning calorimetry (DSC) measurements. In **Figure 2**, we compare XRD patterns (panel a) and DSC measurements (panel b) of samples annealed for 0 and 24 days. Although the glass is held at temperatures well above its glass transition for several tens of minutes during preform consolidation and fiber drawing, the XRD pattern of the as-drawn fiber shows only halos of diffraction indicative

[*] Dr. S. Danto, Dr. F. Sorin, Dr. N. D. Orf, Dr. Z. Wang, Prof. Y. Fink
Department of Materials Science and Engineering
Massachusetts Institute of Technology (MIT)
Cambridge, MA 02139 (USA)
E-mail: yoel@mit.edu
Dr. S. Danto, Dr. F. Sorin, Dr. N. D. Orf, Dr. Z. Wang,
Prof. J. D. Joannopoulos, Prof. Y. Fink
Research Laboratory of Electronics
MIT, Cambridge, MA 02139 (USA)
Dr. S. A. Speakman
Center for Materials Science and Engineering
MIT, Cambridge, MA 02139 (USA)
Prof. J. D. Joannopoulos, Prof. Y. Fink
Institute for Soldier Nanotechnologies
MIT, Cambridge, MA 02139 (USA)

DOI: 10.1002/adma.201000268

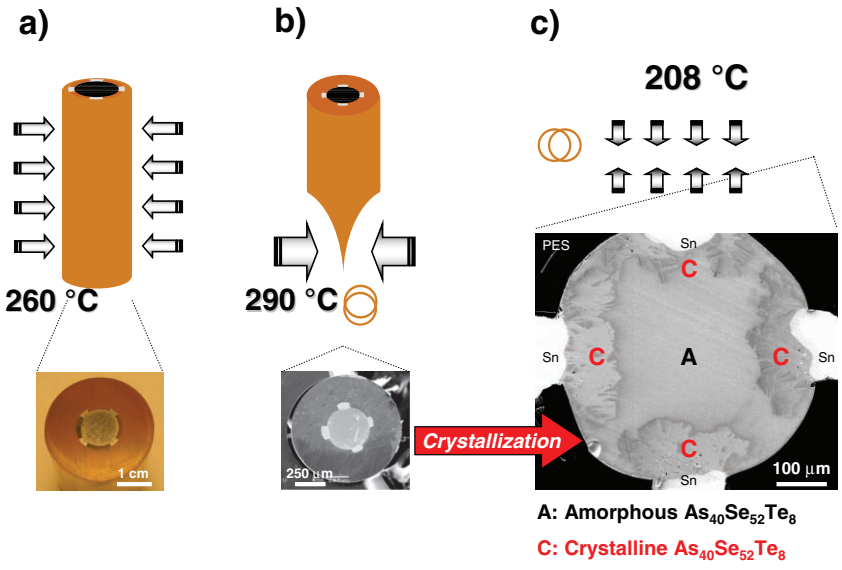

Figure 1. Fiber device fabrication. The preform consists of an amorphous core of $As_{40}Se_{52}Te_8$ contacted by four Sn electrodes and encapsulated inside a high-T_g PES polymeric cladding. **a)** The preform is consolidated into a single structure at 260 °C for ~30 minutes and **b)** then drawn to millimeter-scale fibers at ~290 °C. **c)** Extended annealing at 208 °C induces crystallization of the $As_{40}Se_{52}Te_8$ core, starting at the interfaces with the electrodes and polymer and spreading inward (SEM image: 208 °C / 40 days).

of an amorphous material (Figure 2a). In contrast, the XRD pattern of the annealed fiber shows a superposition of diffuse halos and sharp crystallographic peaks typical of a glass-ceramic. Peak indexation verifies the presence of a crystalline phase isostructural to monoclinic α-$As_{40}Se_{60}$. This result is consistent with previous studies which show that selenium is continuously replaced by tellurium for Te concentrations less than 10% in the $As_{40}[Se_{1-x}Te_x]_{60}$ system, resulting in single phase solutions.[11] The SEM image also reveal that the growth of the crystalline phase inside the $As_{40}Se_{52}Te_8$ region begins at the interfaces between the glass and the electrodes and polymer cladding before extending into the bulk. While electron-probe microanalysis shows no sign of tin diffusion into the semiconductor core, we suspect that the preferential destabilization of the glass at its interface with the electrodes is activated through a mechanism of catalyzed crystallization by Sn.[12,13] The

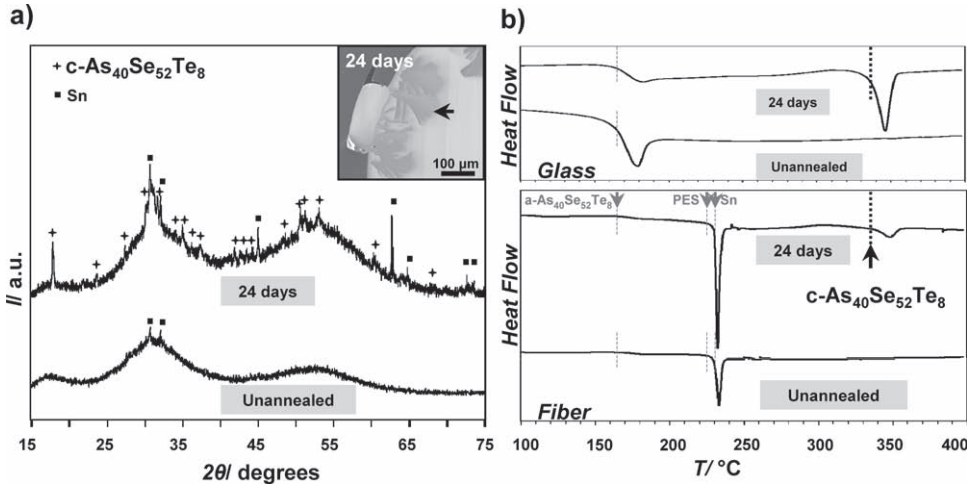

Figure 2. Characterization of crystalline semiconductor domains. **a)** XRD patterns of unannealed and annealed (24 days) fibers. A crystalline phase (c-$As_{40}Se_{52}Te_8$) isostructural to α-$As_{40}Se_{60}$ grows inside the glassy matrix with extended annealing (inset: SEM image of a fiber cross-section annealed for 24 days, arrow highlight crystalline domains). **b)** DSC scans of $As_{40}Se_{52}Te_8$ glass (upper panel) and multimaterial fiber (lower panel). Annealing of both glass and fiber for 24 days leads to the presence of an exothermal peak at T_m = 338 °C associated with the melting of crystalline $As_{40}Se_{52}Te_8$.

partial crystallization of the semiconductor is further supported by DSC measurements (Figure 2b). In Figure 2b (upper panel), the unannealed glass exhibits a single characteristic temperature (T_g = 165 °C) while the annealed glass shows an additional melting peak at T_m = 338 °C, suggesting that a crystalline phase exists within the glassy matrix. In Figure 2b (lower panel), DSC scans of complete sections of both as-drawn and annealed fibers show the characteristic thermal parameters of the three constituting components: the glass transition temperatures of $As_{40}Se_{52}Te_8$ and PES (165 and 225 °C, respectively) and the melting temperature of Sn at 232 °C. The annealed fiber exhibits an additional endothermic peak at 338 °C, matching exactly with the melting temperature of the crystalline $As_{40}Se_{52}Te_8$ phase. Hence, while the thermal drawing process does not initiate crystallization of the $As_{40}Se_{52}Te_8$ alloy, annealing of drawn fiber at 208 °C can induce significant crystallization.

To better understand the devitrification process, we investigated the crystallization kinetics of glassy $As_{40}Se_{52}Te_8$ using the Johnson–Mehl–Avrami model (**Figure 3a**).[14–16] The three characteristic parameters of the phase transformation, namely the activation energy E_a, the Avrami exponent n and the pre-exponential frequency factor k_o, were determined under isothermal conditions via DSC. The crystallized fraction as a function of time, α, of the $As_{40}Se_{52}Te_8$ glass was recorded in the range 270–310 °C where scans could be recorded on acceptable time scales. The kinetics of phase transformation under isothermal conditions is described by the Avrami equation:

$$\alpha = 1 - \exp[-(k(t)^n] \quad (1a)$$

or by the equivalent relation:

$$\ln[-\ln(1-\alpha)] = n \ln t + n \ln k \quad (1b)$$

where α is the crystallized fraction at time t and k is the kinetic rate constant at absolute temperature T. The kinetic rate constant k is defined by an Arrhenius relation of the form:

$$k(T) = k_0 \exp\left[-\frac{E_a}{k_B.T}\right] \quad (2)$$

where k_B is the Boltzmann constant. In agreement with Equation (1b), the plot of ln[-ln(1-α)] against ln t at constant temperatures yields a linear relation from which n and $k(T)$ were extracted. The Avrami exponent n was found to be in the range 2.02 –2.36. The activation energy of the reaction E_a = 0.89 eV and the pre-exponential frequency k_0 = 4.36 10^3 s^{-1} were calculated from Equation (2). The crystallized fraction of the $As_{40}Se_{52}Te_8$ glass against time was then extrapolated at 208 °C from Equation (1) using the averaged value $\langle n \rangle$ = 2.2. The glass requires a few hours to reach its complete crystallization in the range 270 – 310 °C but upwards of 10 months when held at 208 °C (Figure 3a). In Figure 3a (inset), the calculated phase transformation ratio of the glass is shown with the experimentally measured ratio for both undrawn bulk and fiber-drawn pieces (see Experimental Section). We interpret the slight deviation between the calculated and measured ratios of the undrawn glass chunk sample as a variation with temperature of the Avrami exponent (best fit at 208 °C: n = 1.9 instead of $\langle n \rangle$ = 2.2). Note that the fiber-drawn glass crystallizes approximately three times faster than the bulk glass. This is likely due to the combination of ordering produces by the fiber drawing process and the increase in the glass-polymer and glass-electrode surface area, enhancing crystallization through an initial heterogeneous nucleation and growth mechanism.

Electrical conductivity measurements also reveal structural changes in the semiconductor. As illustrated in Figure 3b (curve shown in black), we observe a 5 to 6 order-of-magnitude decrease in series resistance of the solid-core fiber devices as the crystal phase extends inside the amorphous matrix with annealing. This decrease largely happens over the course of 3 days after 2 days of incubation. SEM images show that during these 5 days, heterogeneous crystallization initiates at the surface of the glass, inducing dramatic drops in resistance as crystalline high conductivity channels ultimately connect the tin electrodes. Further crystalline domains growth into the bulk

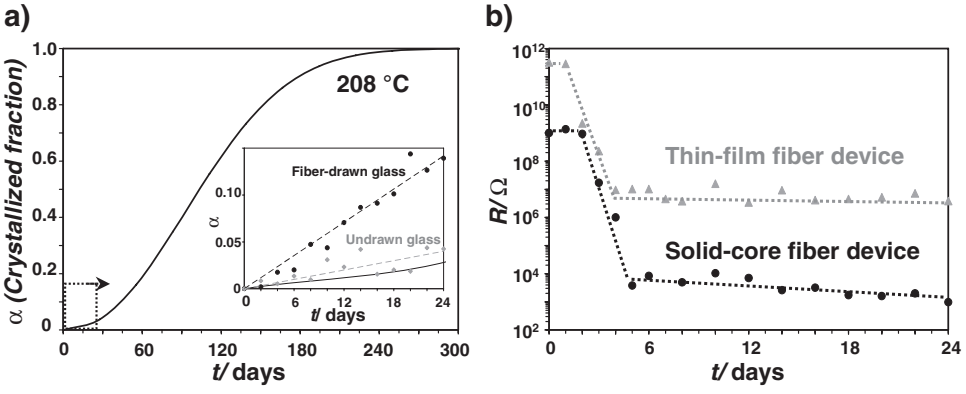

Figure 3. a) Crystallization kinetics of the $As_{40}Se_{52}Te_8$ glass. The transformed fraction of the glass is extrapolated at 208 °C using the Avrami relation (inset: calculated crystallization rate versus experiment, evaluated by DSC for both undrawn glass chunk and fiber-drawn samples). **b)** Time-evolution of the electrical resistance of both solid-core and thin-film fiber devices. Measurements are made between two adjacent Sn electrodes at room temperature and in the dark ($l_{Fib.}$ = 15 cm, $\Phi_{Fib.}$ ~ 1.30 mm). As the crystal phase extends inside the amorphous matrix, the fiber devices exhibit a 5 to 6 order-of-magnitude decrease in the electrical resistance.

shows little impact on the conductivity, as a low resistance channel has already been established.

We now turn to an alternative geometry: replacing the solid core with a thin-film photoconducting structure. A striking advantage of a thin-film structure compared to its solid-core counterpart is the significant reduction of dark current and hence device noise per unit length.[6] The electrical resistance with annealing of such thin-film fiber devices exhibits a similar behavior (Figure 3b, curve shown in gray). In this case, the maximal conductivity is reached within only 4 days. Thin-film fiber devices have twice as much surface area contact between glass and cladding, increasing the crystal nucleation and growth rate. For both devices, post-drawing crystallization of the glass induces reorganization of the crystallographic structure toward a more ordered one with significantly fewer dangling bonds. This drastically reduces the density of localized states inside the band-gap of the semiconductor film, increases carrier mobility, and enhances the glass conductivity.[17,18]

The formation of crystalline semiconductor domains within multimaterial fibers enables active electric devices to be constructed. As a proof-of-concept, we demonstrate the first single-fiber p-channel field-effect device with a source-to-drain conductance controlled by an applied gate voltage. The structure consists of two identical thin film devices, each made of the p-type $As_{40}Se_{52}Te_8$ semiconductor functioning as the channel and contacted by two parallel Sn electrodes acting as the source and the drain (**Figure 4a**). A third Sn electrode is used as the gate and is separated from the channel by a PES dielectric layer. This fiber device, designed to operate in accumulation mode, was prepared and annealed at 208 °C. As can be seen in Figure 4b (upper panel), after annealing for 14 days the source-to-drain current I_{DS} shows a strongly nonlinear dependence on the applied gate voltage V_G under fixed V_{DS}. Steady state is reached after a transient time of several minutes due to the presence of remaining defect states into the semiconductor.[19] In contrast, identical non-annealed fiber structures have extremely low channel conductivity and show no dependence on the gate voltage. In Figure 4b (lower panel), the source-to-drain current – voltage characteristics demonstrate a clear increase in the conductance of the channel as the gate bias is varied from 0 V to −100 V. In this proof-of-concept, the transistor suffers from fabrication limitations that keep its performance below that required for circuitry. For example, reducing the thickness of the gate dielectric through structural and fabrication optimizations would lower the present current turn-on voltage (V_G ~ −75 V to observe an on-to-off I_{DS} current ratio of 100%). Also, matching source-to-drain and gate electrode lengths would alleviate contact resistance effects. Nevertheless, a clear current

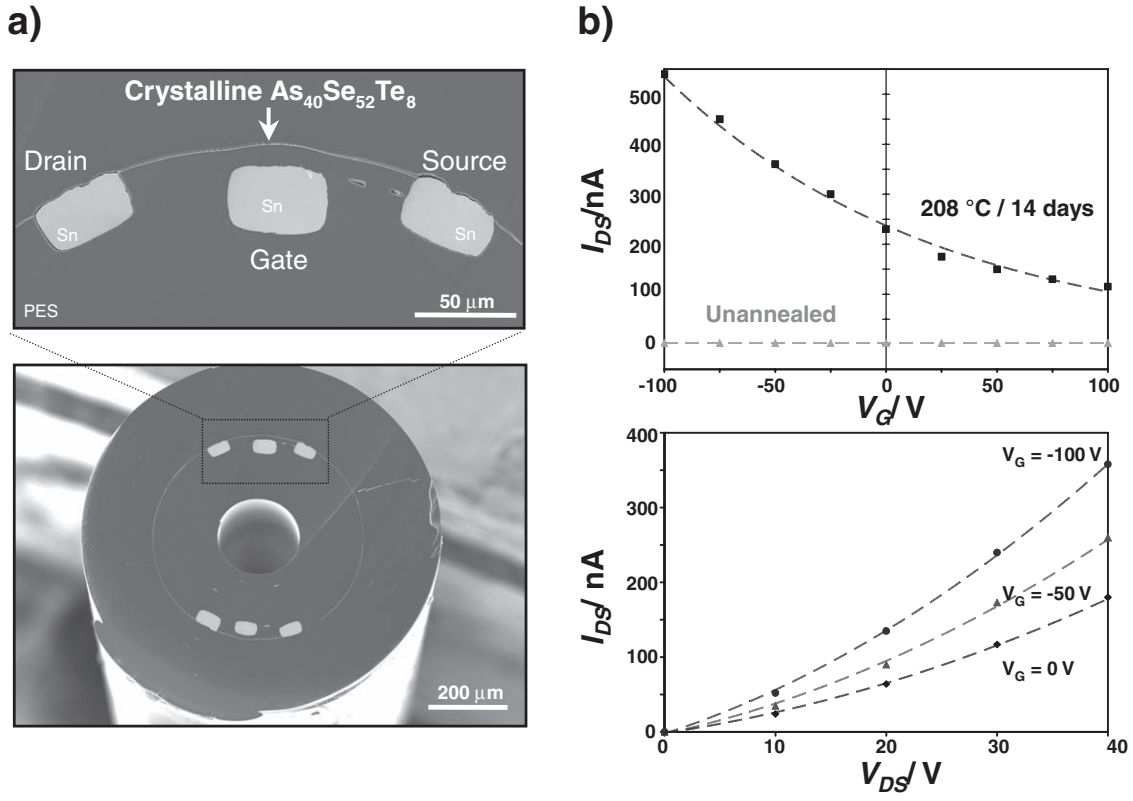

Figure 4. Fiber field-effect device. **a)** SEM image of the cross-section of the fiber device whole structure (lower panel). Magnification of one of the two devices (upper panel). Two parallel source and drain Sn electrodes are in contact with the p-type $As_{40}Se_{52}Te_8$ film. A third Sn electrode separated from the channel by an insulating PES polymer film functions as the gate electrode. **b)** Characterization of the field-effect device. Drain-to-source current I_{DS} as a function of the gate voltage V_G for unannealed and 14 days annealed fibers (V_{DS} = 20 V) (upper panel). Source-to-drain I_{DS} – V_{DS} characteristics of the field-effect device as function of the gate voltage (lower panel).

modulation in the crystalline devices is demonstrated. It reveals the unpinning of the Fermi level resulting from a more ordered crystallographic structure. Assuming the device is operating in the linear regime (and underestimated due to the effect of contact resistances), the mobility of the c-$As_{40}Se_{52}Te_8$ semiconductor in the FET device is found to be ~1.50 10^{-2} cm^2 V^{-1} s^{-1}, a substantial increase over the amorphous state ($\mu_{a\text{-}As2Se3}$ ~ 5.00 10^{-5} cm^2 V^{-1} s^{-1}[20]). This result demonstrates the profound impact of the *in situ* crystallization on electrical properties of the incorporated semiconductor.

In this paper we demonstrate, for the first time, the integration inside a fiber device of a phase-changing glassy semiconductor compatible with thermal drawing. This result makes it possible to modulate in situ the electrical properties of semiconducting elements. Further developments are envisioned to reduce phase-change time from days to minutes and even seconds to ultimately crystallize the glass during drawing. One approach consists of using increasingly unstable glass compositions. Optically-induced crystallization methods are another promising route towards the fabrication of crystalline domains in multimaterial device fibers.[2] The reduction in defect density and corresponding drop in resistivity is expected to create unprecedented opportunities in the design of more and more complex electric devices into fiber. As a proof-of-concept, we fabricated the first meters-long single-fiber field-effect device. With an increase of both the number of incorporated transistors and their performance, it is easy to imagine creating in fiber devices discrete logic elements capable of digital signal processing, opening a whole new area of applications for optoelectronic and electronic.

Experimental Section

Amorphous semiconductor synthesis: The amorphous semiconductor $As_{40}Se_{52}Te_8$ was prepared from high-purity As, Se and Te elements (Alfa Aesar, 5–6N) by the standard melt-quench method. Pieces of As, Se and Te were introduced into a quartz ampoule and placed under vacuum (~10^{-5} Torr). The quartz tube was then sealed and heated in a rocking furnace to 750 °C for 12 h to assure complete homogenization of the melt. The ampoule was quenched in water, annealed at 165 °C for 2 h and cooled to room temperature.

Preform preparation and fiber drawing: Solid-core fiber device preforms were prepared by sliding a $As_{40}Se_{52}Te_8$ glass rod of 10-mm diameter into a polymer tube having four slots cut out. Tin electrodes were inserted into the slots and additional polymer was wrapped around the metal-semiconductor device until the final preform diameter was ~27 mm. Thin-film fiber devices were fabricated by thermal evaporation of bulk $As_{40}Se_{52}Te_8$ onto a 75-µm polymer film. The film was then rolled around a polymer tube and the whole structure was encapsulated in an additional electrode tube and polymer cladding as above. Field-effect device preforms were prepared using similar techniques. The preforms were consolidated under vacuum at 260 °C for ~30 min and then drawn at ~290 °C in a standard fiber draw tower. With this procedure, ~25 meters of fiber were drawn with diameters ranging from 0.80 mm to 1.40 mm.

Fiber device characterization: The XRD characterization of solid-core fiber was performed with a Rigaku Powder Diffractometer (Cu target, λ = 1.54056 Å). Prior to XRD analysis, the outer PES layer of the fibers was dissolved with N, N-dimethylacetamide, the electrodes were stripped and the remaining semiconductor was crushed into powder. The thermal characterization was carried out with a Q1000 TA instruments DSC (heating rate: 10 °C min^{-1}). The characteristic temperatures were taken to be the onset of the thermal event. In order to evaluate the crystallization fraction of the $As_{40}Se_{52}Te_8$ glass over time, both undrawn glass pieces and fiber-drawn samples were annealed at 208 °C. Prior to the DSC scans of fiber samples, the outer PES cladding and the Sn electrodes were removed.

The electrical measurements were performed with a Keithley 6517a electrometer and 6487 picoammeter. Samples of similar geometry (l_{Fib} = 15 cm, Φ_{Fib} ~ 1.30 mm) were selected. Electrical contacts were made to the tin electrodes by stripping away the PES cladding and attaching thin wires to the exposed electrodes with conductive Ag paint. Measurements were made in the dark at room temperature.

Acknowledgements

The authors thank N. Chatterjee for technical assistance. This work was supported in part by the Materials Research Science and Engineering Program of the US National Science Foundation under award number DMR-0819762, and also in part by the US Army Research Office through the Institute for Soldier Nanotechnologies at MIT under contract no. W911NF-07-D-0004. We also thank the RLE and CMSE for their support.

Received: January 22, 2010
Published online: August 20, 2010

[1] B. Bureau, X. H. Zhang, F. Smektala, J. L. Adam, J. Troles, H. L. Ma, C. Boussard-Pledel, J. Lucas, P. Lucas, D. Le Coq, M. R. Riley, J. H. Simmons, *J. Non-Cryst. Solids* **2004**, *345*, 276.
[2] M. Wuttig, N. Yamada, *Nat. Mater.* **2007**, *6*, 824.
[3] M. Bayindir, F. Sorin, A. F. Abouraddy, J. Viens, S. D. Hart, J. D. Joannopoulos, Y. Fink, *Nature* **2004**, *431*, 826.
[4] A. F. Abouraddy, O. Shapira, M. Bayindir, J. Arnold, F. Sorin, D. Saygin-Hinczewski, J. D. Joannopoulos, Y. Fink, *Nat. Mater.* **2006**, *5*, 532.
[5] A. F. Abouraddy, M. Bayindir, G. Benoit, S. D. Hart, K. Kuriki, N. Orf, O. Shapira, F. Sorin, B. Temelkuran, Y. Fink, *Nat. Mater.* **2007**, *6*, 336.
[6] F. Sorin, A. F. Abouraddy, N. Orf, O. Shapira, J. Viens, J. Arnold, J. D. Joannopoulos, Y. Fink, *Adv. Mater.* **2007**, *19*, 3872.
[7] F. Sorin, O. Shapira, A. F. Abouraddy, M. Spencer, N. D. Orf, J. D. Joannopoulos, Y. Fink, *Nano Lett.* **2009**, *9*, 2630.
[8] A. A. Vaipolin, E. A. Porai-Koshits, *Sov. Phys. Solid State* **1963**, *5*, 186.
[9] M. H. El-Fouly, J. T. Edmond, *Phys. Status Solidis A* **1974**, *21*, 43.
[10] R. E. Loehman, A. J. Armstrong, *J. Am. Ceram. Soc.* **1977**, *60*, 71.
[11] M. F. Kotkata, M. Shamah, M. B. El-Den, M. K. El-Mously, *Acta Phys. Hung.* **1983**, *54*, 49.
[12] J. J. Cheng, J. Zarzyckia, J. C. Jumasc, M. Ribesc, *J. Non-Cryst. Solids* **1981**, *45*, 47.
[13] J. J. Cheng, G. Tilloga, J. Zarzycki, *J. Non-Cryst. Solids* **1982**, *52*, 249.
[14] W. A. Johnson, R. F. Mehl, *Am. Inst. Mineral. Metall. Eng.* **1939**, *135*, 416.
[15] M. Avrami, *J. Phys. Chem.* **1939**, *7*, 1103.
[16] M. Avrami, *J. Phys. Chem.* **1939**, *8*, 212.
[17] A. A. Abu-Sehly, M. I. Abd-Elrahman, *J. Phys. Chem. Solids* **2002**, *63*, 63.
[18] A. S. Soltan, M. Abu El-Oyoun, A. A. Abu-Sehly, A. Y. Abdel-Latief, *Mater. Chem. Phys.* **2003**, *82*, 101.
[19] R. C. Frye, D. Adler, *Phys. Rev. B* **1981**, *24*, 5812.
[20] A. I. Lakatos, M. Abkowitz, *Phys. Rev. B Condens. Matter Mater. Phys.* **1971**, *3*, 1791.